

Ground state and persistent oscillations in the quantum East model

Adway Kumar Das* and Achilleas Lazarides†

School of science, Loughborough University, Loughborough, Leicestershire LE11 3TU, UK

(Dated: March 2, 2026)

For the 1D quantum East model with open boundaries, we show that in the limit $s \rightarrow -\infty$, the ground state is accurately captured by a simple spin-coherent product state. We further identify a low-entanglement excited eigenstate that differs from the ground state only by a π -rotation of the boundary spin, remaining well approximated by a spin-coherent state. For a range of $-\infty < s < 0$, the edge-coherent product state overlaps with two eigenstates separated by a size-independent energy gap, leading to persistent coherent oscillations of both global and local observables in the thermodynamic limit. These oscillations originate from boundary physics and are distinct from quantum many-body scars or hypercube-like Fock-space mechanisms.

Thermalization and its breakdown in closed quantum systems is a fascinating area of research [1–11]. In case of ergodic systems, excited eigenstates extend throughout Hilbert space [12–15] and local observables equilibrate at long times to the Gibbs ensemble.

One counterexample is many-body localisation (MBL), which occurs in systems with quenched disorder where emergent local conserved quantities prevent thermalisation [16–22]. Recently, the stability of the MBL phase in the thermodynamic limit is currently under intense scrutiny [23–29].

A natural question is whether MBL-type physics can occur in translationally invariant systems [30–37]. This question has motivated various kinetically constrained spin-chains without quenched disorder [36–44]. Perhaps the prototypical example is the East model where the Hamiltonian can flip a spin of a Fock state only if its neighbor is in a facilitating configuration [33, 35, 45]. This model exhibits a quantum phase transition (QPT) at $s = 0$ [45–47] where s is the parameter controlling the strength of spin-flips and corresponds to activity in the classical analogue [33]. For $s < 0$, local observables exhibit ballistic spreading and entanglement entropy grows as typically observed in ergodic systems [35]. For $s > 0$, local perturbations spread logarithmically with a relaxation time growing exponentially with the system size [35, 48] and many initial states show slow entanglement growth [49].

Here, we focus on the 1D East model with open boundary conditions, which displays a QPT at $s = 0$ [45, 48]. We first study the limit $s \rightarrow -\infty$, where we find an accurate analytical approximation to the ground state $|\text{GS}\rangle$ and to a special higher-energy, low-entropy eigenstate which we denote $|\text{ES}_1\rangle$ (Fig. 1(a)) lying above it—this state differs from the $|\text{GS}\rangle$ only by a single spin rotation at the rightmost edge of the system. Both of these approximations are spin-coherent states (Eq. (3)), locally correlated and with vanishing entanglement, with the $|\text{ES}_1\rangle$ being an edge mode in that it differs from the $|\text{GS}\rangle$ only at the very edge. We then study the region $-\infty < s < 0$, where we find that $|\text{GS}\rangle$ remains approximately of the same form (see Fig. 1(b) where the overlap

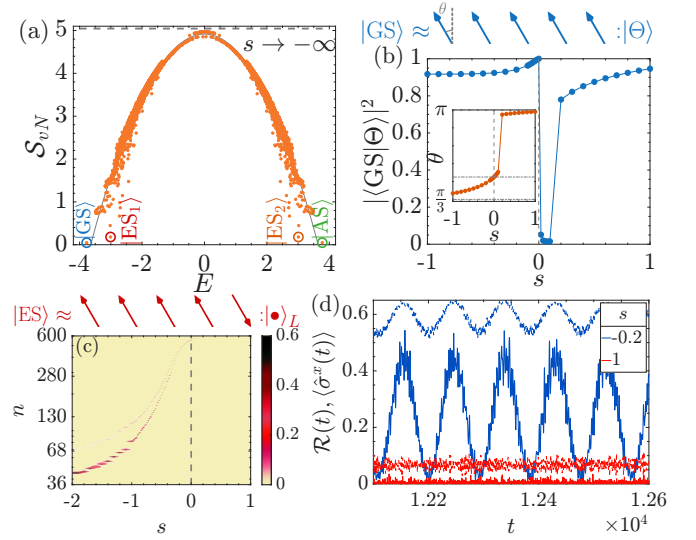


FIG. 1. (a) Bipartite entanglement entropy of energy eigenstates for $L = 16$ and $s \rightarrow -\infty$ (Eq. (2)). The dashed line denotes the Page value. Circles mark the ground state ($|\text{GS}\rangle$), anti-ground state ($|\text{AS}\rangle$), excited states, $|\text{ES}_1\rangle$ and $|\text{ES}_2\rangle$ with unusually low entanglement compared to its neighboring states. (b) Plot shows the overlap of $|\Theta\rangle$ (Eq. (4)) with $|\text{GS}\rangle$ as a function of s for $L = 18$. Inset shows the optimum angle of the individual spins of $|\Theta\rangle$. Above it is a cartoon of $|\Theta\rangle$ approximating $|\text{GS}\rangle$ for $s \leq 0$. (c) Plot shows the overlap of $|\bullet_L\rangle$ with eigenstates ordered in energy (n is the index) for $L = 14$. Colorbar denotes $|\langle \Psi_n | \bullet_L \rangle|^2$. Note how $|\bullet_L\rangle$ for negative-enough s mainly overlaps a single eigenstate, consistent with it being itself an eigenstate at $s \rightarrow -\infty$, while it overlaps strongly with two eigenstates for $s < 0$, leading to the oscillatory dynamics in panel (d). Above is a cartoon of the spin-coherent state, $|\bullet_L\rangle$ which approximates the eigenstate $|\text{ES}_1\rangle$ and differs from $|\text{GS}\rangle$ (see panel (b)) at a single edge spin. (d) Time evolution of survival probability (solid lines) and magnetization along X-direction (dashed lines) for different values of s and $L = 14$ where the initial state is $|\bullet_L\rangle$.

of our ansatz with the $|\text{GS}\rangle$ is shown) while the spin-coherent state eventually (for $-1 \lesssim s \lesssim 0$) develops overlaps with two eigenstates with a system size-independent energy gap between them (Fig. 1(c)). This implies that the low-entanglement state displays long-lived coherent

oscillations of both global (return probability) and local (magnetisation) quantities, which we display in Fig. 1(d).

Our model has the following irreducible Hamiltonian [45]

$$\hat{H}_{\text{East}} = \frac{\hat{\mathbb{I}} + \hat{N}}{2} - \frac{e^{-s}}{2} \left(\hat{\sigma}_1^x + \sum_{j=1}^{L-1} \hat{n}_j \hat{\sigma}_{j+1}^x + \hat{n}_L \right) \quad (1)$$

where $\hat{\sigma}_j^{x,y,z}$ are the Pauli operators, \hat{n}_j is the number density operator $\hat{n}_j = (1 - \hat{\sigma}_j^z)/2$ and $\hat{N} \equiv \sum_{j=1}^L \hat{n}_j$. The two single-spin terms inside the brackets and the $\hat{\mathbb{I}}/2$ are due to the edges, while the $\hat{N}/2$ term is a chemical potential term $\mu \sum_j n_j$ where we set $\mu = 1$ [35].

We begin our study at the limit $s \rightarrow -\infty$, where the Hamiltonian in Eq. (1) reduces to

$$\hat{H}_{-\infty} = -\hat{\sigma}_1^x - \sum_{j=1}^{L-1} \hat{n}_j \hat{\sigma}_{j+1}^x - \hat{n}_L. \quad (2)$$

Figure 1(a) shows the bipartite von Neumann entanglement entropy [15, 20, 50] of the eigenstates of $\hat{H}_{-\infty}$ as a function of energy for $L = 16$, which has a rainbow shape typical of interacting many-body systems, with the exception of a pair of peculiar excited states (marked by circles) with entanglement much lower than their neighbors. These special excited states, denoted by $|\text{ES}_1\rangle$ and $|\text{ES}_2\rangle$, are closely related to the ground state as we will show.

To characterize the structure of the ground state $|\text{GS}\rangle$ in the Fock space, we compute the fractal dimensions D_q from the scaling of the q th moments of its wavefunction intensities [51–54]. For ergodic states $D_q = 1$ for all q while localized states have $D_q = 0$; generally, D_q decreases monotonically with q and so is bounded below by D_∞ [55–57]. In the Z -basis we find $0 < D_q^z < 1$, decreasing with q , with finite $D_\infty^z \approx 0.47$ [58], indicating that $|\text{GS}\rangle$ is multifractal: it occupies an extensive yet vanishing fraction of Hilbert space, with distinct scaling exponents for different moments [12, 59–61]. Multifractality is also present in the X -basis, but with $D_q^x > D_q^z$ for all $q > 0$, implying greater delocalization in the Z -basis. This contrasts with the $s \rightarrow \infty$ limit, where the ground state $|0\rangle^{\otimes L}$ is localized in Z and fully extended in X ($D_q^x = 1$ for all $q > 0$).

In real space, local observables such as $\langle \hat{n}_j \rangle$ and $\langle \hat{\sigma}_j^x \rangle$ are approximately uniform across the chain [58], despite the multifractality in Fock space. The bipartite entanglement entropy remains small and essentially independent of system size, $\mathcal{S}_{vN} \approx 0.0472$, consistent with an area law as expected for the ground state of a local Hamiltonian, but here coexisting with nontrivial multifractality in the configuration space.¹

Overall, then, $|\text{GS}\rangle$ has low entanglement entropy and is nonergodic in Fock space but extended in the real space. This leads us to conjecture that the $|\text{GS}\rangle$ is approximated by a spin-coherent state:

$$|\{\theta_j\}\rangle = \otimes_{j=1}^L |\theta_j\rangle, \quad |\theta_j\rangle = \cos \frac{\theta_j}{2} |1\rangle + \sin \frac{\theta_j}{2} |0\rangle. \quad (3)$$

The energy of the above state w.r.t. the Hamiltonian in Eq. (2) is

$$E_{\{\theta_j\}} = -\sin \theta_1 - \sum_{j=1}^{L-1} \frac{1 + \cos \theta_j}{2} \sin \theta_{j+1} - \frac{1 + \cos \theta_L}{2}.$$

This is minimized by $\theta_j \approx \frac{\pi}{3}$ for all j and L ; this is straightforward to see in the case of periodic boundary conditions, where choosing $\theta_j = \theta$ gives an energy $-\frac{L}{2} \sin \theta (1 + \cos \theta)$, minimized at $\theta = \frac{\pi}{3}$. Thus, the ground state is well-approximated by the ansatz

$$|\text{GS}\rangle_{s \rightarrow -\infty} \approx |\Theta\rangle \equiv \left| \frac{\pi}{3} \right\rangle^{\otimes L}. \quad (4)$$

The energy of this state is a good approximation to that of the exact $|\text{GS}\rangle$ [58] for all accessible system sizes. Furthermore, extrapolating the overlap of this ansatz with the $|\text{GS}\rangle$ gives $\lim_{L \rightarrow \infty} |\langle \text{GS} | \Theta \rangle|^2 \approx 0.5862 \pm 0.0394$, so that the overlap remains finite. The deviation of the real $|\text{GS}\rangle$ is reflected in the low, L -independent value of the entanglement entropy of the $|\text{GS}\rangle$.

Additionally, our ansatz reproduces all the qualitative features of the ground state: $\langle \frac{\pi}{3} | \hat{n} | \frac{\pi}{3} \rangle = \frac{3}{4}$ and $\langle \frac{\pi}{3} | \hat{\sigma}^x | \frac{\pi}{3} \rangle = \frac{\sqrt{3}}{2}$, both of which are close to the expectation values w.r.t. the ground state [47]. We analytically obtain the fractal dimensions of $|\Theta\rangle$ [58]

$$D_q^z = \frac{\log_2(1 + 3^q) - 2q}{1 - q} \quad (5)$$

$$D_q^x = \frac{\log_2(\sqrt{3} + 1)^{2q}(1 + (\sqrt{3} - 2)^{2q}) - 3q}{1 - q}$$

which are consistent with the ground state being more delocalized over the Z -basis compared to X -basis. They are the same for the $|\text{ES}_1\rangle$ state and also in good agreement with exact results for that (see Fig. 2(c)).

Dynamical support for the strong overlap of the spin-polarized ansatz with the ground state is furnished by studying its survival probability

$$\mathcal{R}(t) \equiv \left| \langle \Theta | \Theta(t) | \Theta \rangle \right|^2, \quad |\Theta(t)\rangle = e^{-iHt} |\Theta\rangle. \quad (6)$$

¹ We note that our numerical results cannot exclude a logarithmic

dependence of \mathcal{S}_{vN} on L , but this does not affect our conclusions.

In ergodic systems, $\mathcal{R}(t)$ typically relaxes to a plateau after the Heisenberg time $t_H \sim 1/\delta$ [60, 62–67] with δ the mean level spacing. Here, however, $\mathcal{R}(t)$ remains $\mathcal{O}(1)$ even for $t \gtrsim t_H$ (with $t_H \sim \mathcal{O}(\sqrt{L})$), reflecting that $|\Theta\rangle$ has $\mathcal{O}(1)$ overlap with the true ground state [58]. This is in complete agreement with our previous picture of the $s \rightarrow -\infty$ ground state as a tilted collective spin.

In conclusion, the ground state in the $s \rightarrow -\infty$ limit is well-approximated by a spin-coherent state, which is the first important result of this Letter. We now use this result to obtain the anti-ground state.

As $\hat{H}_{-\infty}$ contains terms with an odd number of σ^x operators, it anti-commutes with the Z parity operator $\hat{P} = \otimes_j \hat{\sigma}_j^z$, $\{\hat{H}, \hat{P}\} = 0$. This chiral symmetry causes spectral pairing: if $\hat{H}|\Psi_n\rangle = E_n|\Psi_n\rangle$, then $\hat{P}|\Psi_n\rangle$ is an also an eigenstate with energy $-E_n - 1$.² Applying \hat{P} to our ansatz for the ground state, $|\frac{\pi}{3}\rangle^{\otimes L}$, yields $|\frac{5\pi}{3}\rangle^{\otimes L}$ as an approximation to the anti-ground state. Compared to the ansatz for the |GS), this state has the opposite X -magnetisation and the same fractal dimensions, and it retains finite overlap³ with the true anti-ground state in the thermodynamic limit: $\lim_{L \rightarrow \infty} |\langle \text{AS} | \frac{5\pi}{3} | \text{AS} | \frac{5\pi}{3} \rangle^{\otimes L}|^2 \approx 0.4040 \pm 0.0272$.

We now extend our study of the |GS) to finite $s > -\infty$. At the QPT point $s = 0$ (the Rokhsar-Kivelson point [35, 68]), the ground state is $|+\rangle^{\otimes L}$ with zero energy. For finite s , we obtain the ground state numerically using the wall-Chebyshev projector [69]. For $s > 0$, it is exponentially localized near the first site, with both $\langle \hat{n}_j \rangle$ and $\langle \hat{\sigma}_j^x \rangle$ decaying exponentially in j . For $s < 0$, the corresponding localization lengths diverge and these observables become spatially homogeneous [45, 58]. This localization-delocalization transition in real space signals a first-order QPT at $s = 0$.

Following our approach for $s \rightarrow -\infty$ we again compute the fractal dimensions for various values of s (see Fig. 3(b)) and find that, in the Z -basis, |GS) is localised in Fock space for $s > 0$ and delocalised for $s < 0$ (multifractal in the Z basis). On the other hand, in the X -basis it is delocalised for $s > 0$, consistent with a product state in the Z -basis, while it is multifractal for $s < 0$. The QPT is therefore also reflected in the fractal dimensions.

Seeking an approximation to the |GS) for arbitrary s in the form of Eq. (3), we minimize its energy with $\theta_j = \theta$. For periodic boundary conditions, this is $\frac{1}{2} + \frac{L}{2} \cos^2 \frac{\theta}{2} - \frac{e^{-s}}{4} L \sin \theta (1 + \cos \theta)$. The angle minimising

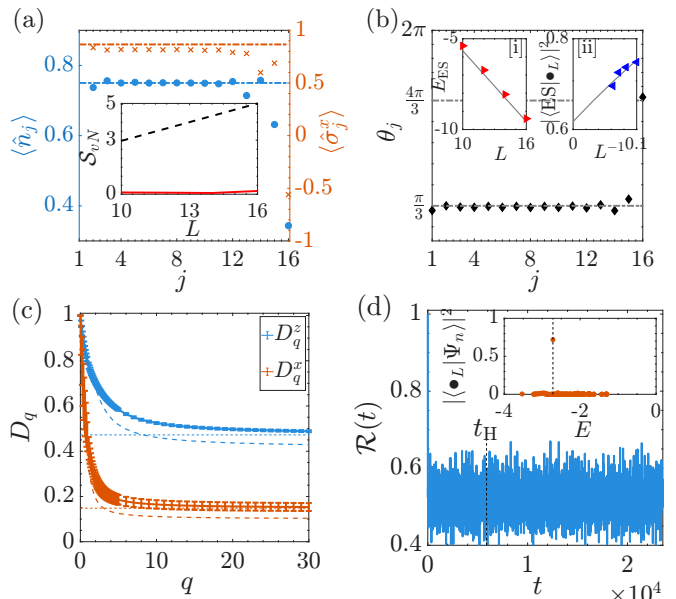


FIG. 2. All panels in this figure for $s \rightarrow -\infty$. (a) Number density and magnetization along X -directions for $|\text{ES}_1\rangle$ (see Fig. 1(a)) versus lattice site for $L = 16$. Horizontal dashed lines denote $\langle \hat{n} \rangle = \frac{3}{4}$ and $\langle \hat{\sigma}^x \rangle = \frac{\sqrt{3}}{2}$, as expected for the spin-polarized state $|\frac{\pi}{3}\rangle^{\otimes L}$. Note that the last lattice site deviates significantly from the dashed lines for both observables. Inset shows the entanglement entropy of $|\text{ES}_1\rangle$ vs. system size where the dashed line denotes the Page values. (b) Optimum angles of a spin-coherent state (Eq. (3)) maximizing the overlap with $|\text{ES}_1\rangle$. Inset [i] shows the energy of the spin-coherent state $|\bullet_L\rangle$ (solid line) and $|\text{ES}_1\rangle$ (markers). Inset [ii] shows the overlap of $|\text{ES}_1\rangle$ with $|\bullet_L\rangle$ as a function of inverse system size along with linear fit (solid line). (c) Fractal dimensions of $|\text{ES}_1\rangle$ in both Z - and X -bases. Horizontal dashed lines denote D_∞ . Error-bars denote 95% confidence interval. (d) Survival probability of the spin-coherent state. Vertical dashed line denotes the Heisenberg time. Inset shows the overlap of the spin-coherent state with the energy eigenstates where the vertical line denotes the energy of $|\text{ES}_1\rangle$.

this for each s is shown in the inset to Fig. 1(b), and the main panel shows the overlap of the ansatz at this angle with the exact |GS). Starting from $\pi/3$ for $s = -\infty$, θ rotates to $\pi/2$ at $s = 0$, with the rotated ansatz remaining a good approximation throughout. It also remains a good approximation for $s > 0$ except for a small region near and above $s = 0$.⁴

We now turn to the excited state $|\text{ES}_1\rangle$ (Fig. 1(a)). In Fig. 2(a), we show that the expectation values of the local observables are homogeneous over the real space except the last site. We also find that the entanglement entropy of $|\text{ES}_1\rangle$, $S_{vN} \approx 0.1090$ is approximately independent of

² It also causes the Fock-space connectivity to be bipartite, so that even and odd parity sectors couple only to each other.

³ Note that $|\frac{5\pi}{3}\rangle$ is not orthogonal to $|\frac{\pi}{3}\rangle$ whereas the true ground state must be orthogonal to the true anti-ground state, both being eigenstates. Nevertheless its overlap with the true anti-ground state is finite.

⁴ The reason that the overlap is very small for $s > 0$ is that that the |GS) becomes exponentially localized in real space and therefore not well captured by our ansatz.

system size and much smaller than the Page value [70].

The low entanglement entropy and difference of local observables on the last lattice site compared to the rest together again suggest an ansatz of the form of Eq. (3). We obtain the angles θ_i by maximising the overlap with $|\text{ES}_1\rangle$ and show the resulting θ_j 's for $L = 16$ in Fig. 2(b). We find that $\theta_i = \theta_1$ for $i = 1 \dots L - 1$ while $\theta_L \neq \theta_1$ so that the $|\text{ES}_1\rangle$ differs from the $|\text{GS}\rangle$ only at the rightmost spin, which is flipped by π . Denoting $|\circ\rangle = |\frac{\pi}{3}\rangle$ and $|\bullet\rangle = |\frac{4\pi}{3}\rangle$,

$$|\text{ES}_1\rangle \approx |\circ\rangle^{\otimes(L-1)} \otimes |\bullet\rangle \equiv |\bullet_L\rangle \quad (7)$$

This state well approximates the energy of $|\text{ES}_1\rangle$ ($\approx \frac{5\sqrt{3}}{8} - \frac{1}{4} - \frac{3\sqrt{3}L}{8}$) for all system sizes, as shown in Fig. 2(b). By a linear fit, we find the overlap between $|\text{ES}_1\rangle$ and $|\bullet_L\rangle$ to be 0.6153 ± 0.1289 in the thermodynamic limit. Thus, even for $L \rightarrow \infty$, the spin-coherent state has a strong ($\sim \mathcal{O}(1)$) overlap with the eigenstate $|\text{ES}\rangle$. As a result, the survival probability starting from $|\bullet_L\rangle$ again does not decay even beyond the Heisenberg time, remaining $\sim \mathcal{O}(1)$, see Fig. 2(d). The fractal dimensions of $|\text{ES}_1\rangle$ are well approximated by Eq. (5), as the fractal dimensions of our ansatz remain the same when approximating both $|\text{GS}\rangle$ and $|\text{ES}_1\rangle$. This shown in Fig. 2(c). The chiral symmetry of $\hat{H}_{s \rightarrow -\infty}$ implies that, $\hat{P}|\bullet_L\rangle = |\frac{5\pi}{3}\rangle^{\otimes(L-1)} \otimes |\frac{2\pi}{3}\rangle$ has a high degree of overlap with the excited eigenstate $|\text{ES}_2\rangle$ having energy $\mathcal{O}(L)$.

Thus, we find that the excited but low-entanglement eigenstate $|\text{ES}_1\rangle$ embedded in a spectrum of highly-entangled eigenstates is close to the spin-coherent state $|\bullet_L\rangle$, which can be regarded as an edge mode [71–75] of the East Hamiltonian at $s \rightarrow -\infty$. To further probe this, we perturb our Hamiltonian with a local operator \hat{O} localised at the edge, $\hat{H} \rightarrow \hat{H} + \hat{O}$. The low energy response of the system is encoded in the retarded Green's function [76]

$$\mathcal{G}^R(\omega) = \langle \text{GS} | \hat{O}^\dagger \frac{1}{\omega + i\eta + E_{\text{GS}} - \hat{H}} \hat{O} | \text{GS} \rangle \quad (8)$$

where η is a small broadening parameter ensuring analytic continuity and E_{GS} is the ground state energy. The presence of an edge mode appears as a pole of the Green's function and so a sharp peak in the spectral function $\mathcal{A}(\omega) = -\frac{1}{\pi} \text{Im} \mathcal{G}^R(\omega)$ such that [77]

$$\mathcal{A}(\omega) \sim \frac{\mathcal{Z}}{\pi} \frac{\Gamma}{(\omega - \omega_0)^2 + \Gamma^2} \quad (9)$$

where ω_0 is the energy, Γ is the inverse lifetime and \mathcal{Z} is the weight of the edge mode. As going from $|\Theta\rangle$ to $|\bullet_L\rangle$ requires applying a π -pulse on the last site around Y-axis, we choose our local perturbation as $\hat{O} = -i\hat{\sigma}_L^y$. In Fig. 3(a), we show that the spectral function $\mathcal{A}(\omega)$ is sharply peaked ($\Gamma \approx 3.0613$) at a constant energy ($\omega_0 \approx 0.8767$) independent of system size. As the spectral width

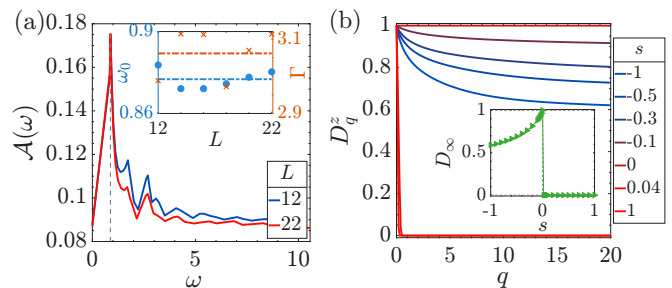


FIG. 3. (a) Spectral function for π -pulse perturbation of the (real) ground state at $s \rightarrow -\infty$. Inset shows the energy (ω_0) and inverse lifetime (Γ) of the edge mode vs. system size obtained from Eq. (9). (b) Fractal dimensions of the $|\text{GS}\rangle$ in Z-basis for different values of s . Inset shows D_∞ vs. s capturing QPT at $s = 0$.

of $\hat{H}_{-\infty}$ scales as $\sim \sqrt{L}$ while ω_0 remains constant, the spectral function shows that $|\bullet_L\rangle$ is an edge mode with the excitation pinned to the last site having long lifetime despite the bulk eigenstates being ergodic [58].

Away from $s = -\infty$, for $s \lesssim -1$ the state $|\bullet_L\rangle$ still has strong overlap with a single eigenstate, while for $-1 \gtrsim s$ it develops appreciable overlap with two eigenstates with different energies, the gap between which is independent of the system size and decreases upon increasing s , vanishing at $s = 0$ (Fig. 1(c)). These overlaps approach finite values in the thermodynamic limit. In other words, for $-1 \gtrsim s \gtrsim 0$, the locally-correlated initial state $|\bullet_L\rangle$ has significant overlap with two eigenstates and results in persistent oscillations. We show this in Fig. 1(d), where the time evolution of both the survival probability (a global observable) and $\langle \hat{\sigma}_x(t) \rangle = \langle \sum_i \hat{\sigma}_i^x(t) \rangle / L$, a local observable, are shown. Let us remark here that the athermal initial state $|\bullet_L\rangle$ is not embedded in the bulk spectrum, but rather remains close (but above and distinct from) the $|\text{GS}\rangle$. The dynamics of the model in Fock space also does not resemble that in a hypercube-like Fock space, as is the case for the PXP model [39]. The persistent oscillations here therefore are not related to the weak ergodicity breaking due to that of the PXP model, forming a distinct class. They also do not appear to be related to those of quantum scars in the semiclassical sense [78].

To summarize, in this Letter, we show that the spin-coherent states successfully capture the low energy physics of the East model at $s \rightarrow -\infty$.

There are several interesting questions to follow up on. Are there other families of states analogous to $|\text{ES}_1\rangle$ that yield long-lived oscillations for suitable initial conditions? Can the mechanism identified here be placed in a broader “scar” framework, either to scars as in [39] or to the many-body version of the semiclassical scar phenomenology as discussed in Ref. [78], or is our $|\text{ES}_1\rangle$ in a fundamentally distinct class? How universal is the phenomenon across kinetically constrained models such

as Fredrickson-Anderson-type models? Finally, how robust are these oscillations to changes in the microscopic dynamics—can they survive in a Floquet/circuit implementation of the constraint, or under Trotterization of Eq. (1)?

We thank J. P. Garrahan and I. M. Khaymovich for many useful discussions. We acknowledge support from the Leverhulme Trust Research Project Grant RPG-2025-063.

* A.K.Das@lboro.ac.uk

† A.Lazarides@lboro.ac.uk

- [1] J. M. Deutsch, *Phys. Rev. A* **43**, 2046 (1991).
- [2] M. Srednicki, *J. Phys. A: Math. Gen.* **32**, 1163 (1999).
- [3] M. Rigol, V. Dunjko, and M. Olshanii, *Nature* **452**, 854 (2008).
- [4] A. M. Kaufman, M. E. Tai, A. Lukin, M. Rispoli, R. Schittko, P. M. Preiss, and M. Greiner, *Science* **353**, 794 (2016).
- [5] K. X. Wei, C. Ramanathan, and P. Cappellaro, *Phys. Rev. Lett.* **120**, 070501 (2018).
- [6] H. Dong, P. Zhang, C. B. Dağ, Y. Gao, N. Wang, J. Deng, X. Zhang, J. Chen, S. Xu, K. Wang, Y. Wu, C. Zhang, F. Jin, X. Zhu, A. Zhang, Y. Zou, Z. Tan, Z. Cui, Z. Zhu, F. Shen, T. Li, J. Zhong, Z. Bao, H. Li, Z. Wang, Q. Guo, C. Song, F. Liu, A. Chan, L. Ying, and H. Wang, *Phys. Rev. Lett.* **134**, 010402 (2025).
- [7] F. Borgonovi, F. Izrailev, L. Santos, and V. Zelevinsky, *Phys. Rep.* **626**, 1 (2016).
- [8] L. D'Alessio, Y. Kafri, A. Polkovnikov, and M. Rigol, *Advances in Physics* **65**, 239 (2016).
- [9] T. Mori, T. N. Ikeda, E. Kaminishi, and M. Ueda, *J. Phys. B: Atom. Mol. Opt. Phys* **51**, 112001 (2018).
- [10] P. Reimann, *Phys. Rev. Lett.* **101**, 190403 (2008).
- [11] N. Linden, S. Popescu, A. J. Short, and A. Winter, *Phys. Rev. E* **79**, 61103 (2009).
- [12] A. De Luca, B. L. Altshuler, V. E. Kravtsov, and A. Scardicchio, *Phys. Rev. Lett.* **113**, 046806 (2014).
- [13] S. Goldstein, J. L. Lebowitz, C. Mastrodonato, R. Tumulka, and N. Zanghì, *Proc. R. Soc. A: Math. Phys. Eng. Sci.* **466**, 3203 (2010).
- [14] J. von Neumann, *EPJ H* **35**, 201 (2010).
- [15] G. De Tomasi and I. M. Khaymovich, *Phys. Rev. Lett.* **124**, 200602 (2020).
- [16] D. M. Basko, I. L. Aleiner, and B. L. Altshuler, *Ann. Phys.* **321**, 1126 (2006).
- [17] A. Pal and D. A. Huse, *Phys. Rev. B* **82**, 174411 (2010).
- [18] R. Nandkishore and D. A. Huse, *Annu. Rev. Condens. Matter Phys.* **6**, 15 (2015).
- [19] M. Serbyn, Z. Papić, and D. A. Abanin, *Phys. Rev. Lett.* **111**, 127201 (2013).
- [20] D. A. Abanin, E. Altman, I. Bloch, and M. Serbyn, *Rev. Mod. Phys.* **91**, 021001 (2019).
- [21] E. Chertkov, B. Villalonga, and B. K. Clark, *Phys. Rev. Lett.* **126**, 180602 (2021).
- [22] A. K. Das, A. Ghosh, and I. M. Khaymovich, *Phys. Rev. Lett.* **131**, 166401 (2023).
- [23] W. De Roeck, F. Huveneers, M. Müller, and M. Schiulaz, *Phys. Rev. B* **93**, 014203 (2016).
- [24] I.-D. Potirniche, S. Banerjee, and E. Altman, *Phys. Rev. B* **99**, 205149 (2019).
- [25] J. Šuntajs, J. Bonča, T. Prosen, and L. Vidmar, *Phys. Rev. E* **102**, 062144 (2020).
- [26] S. Gopalakrishnan and D. A. Huse, *Phys. Rev. B* **99**, 134305 (2019).
- [27] P. T. Dumitrescu, A. Goremykina, S. A. Parameswaran, M. Serbyn, and R. Vasseur, *Phys. Rev. B* **99**, 094205 (2019).
- [28] M. Kiefer-Emmanouilidis, R. Unanyan, M. Fleischhauer, and J. Sirker, *Phys. Rev. B* **103**, 024203 (2021).
- [29] D. Sels and A. Polkovnikov, *Phys Rev E* **104**, 054105 (2021).
- [30] M. Schiulaz, A. Silva, and M. Müller, *Phys. Rev. B* **91**, 184202 (2015).
- [31] Z. Papić, E. M. Stoudenmire, and D. A. Abanin, *Annals of Physics* **362**, 714 (2015).
- [32] N. Y. Yao, C. R. Laumann, J. I. Cirac, M. D. Lukin, and J. E. Moore, *Phys. Rev. Lett.* **117**, 240601 (2016).
- [33] J. P. Garrahan, *Physica A: Statistical Mechanics and its Applications* **504**, 130 (2018).
- [34] M. Schulz, C. A. Hooley, R. Moessner, and F. Pollmann, *Phys. Rev. Lett.* **122**, 040606 (2019).
- [35] M. van Horssen, E. Levi, and J. P. Garrahan, *Phys. Rev. B* **92**, 100305 (2015).
- [36] Z. Lan, M. van Horssen, S. Powell, and J. P. Garrahan, *Physical Review Letters* **121**, 10.1103/physrevlett.121.040603 (2018).
- [37] B. Everest, M. Marcuzzi, J. P. Garrahan, and I. Lesanovsky, *Phys. Rev. E* **94**, 052108 (2016).
- [38] H. Bernien, S. Schwartz, A. Keesling, H. Levine, A. Omran, H. Pichler, S. Choi, A. S. Zibrov, M. Endres, M. Greiner, *et al.*, *Nature* **551**, 579 (2017).
- [39] C. J. Turner, A. A. Michailidis, D. A. Abanin, M. Serbyn, and Z. Papić, *Nature Physics* **14**, 745 (2018).
- [40] J. P. Garrahan, *Physica A: Statistical Mechanics and its Applications* **504**, 130 (2018).
- [41] C. R. Laumann, A. Pal, and A. Scardicchio, *Phys. Rev. Lett.* **113**, 200405 (2014).
- [42] S. Roy and A. Lazarides, *Phys. Rev. Res.* **2**, 023159 (2020).
- [43] P. Brighi and M. Ljubotina, *Phys. Rev. B* **110**, L100304 (2024).
- [44] K. Royen, S. Mondal, F. Pollmann, and F. Heidrich-Meisner, *Phys. Rev. E* **109**, 024136 (2024).
- [45] N. Pancotti, G. Giudice, J. I. Cirac, J. P. Garrahan, and M. C. Bañuls, *Phys. Rev. X* **10**, 021051 (2020).
- [46] J. P. Garrahan, R. L. Jack, V. Lecomte, E. Pitard, K. van Duijvendijk, and F. van Wijland, *Phys. Rev. Lett.* **98**, 195702 (2007).
- [47] M. C. Bañuls and J. P. Garrahan, *Phys. Rev. Lett.* **123**, 200601 (2019).
- [48] H. G. Menzler, M. C. Bañuls, and F. Heidrich-Meisner, *Phys. Rev. B* **112**, 115141 (2025).
- [49] M. Badbaria, N. Pancotti, R. Singh, J. Marino, and R. J. Valencia-Tortora, *PRX Quantum* **5**, 040348 (2024).
- [50] M. Haque, P. A. McClarty, and I. M. Khaymovich, *Phys. Rev. E* **105**, 014109 (2022).
- [51] C. M. Soukoulis and E. N. Economou, *Phys. Rev. Lett.* **52**, 565 (1984).
- [52] A. Rodriguez, L. J. Vasquez, K. Slevin, and R. A. Römer, *Phys. Rev. Lett.* **105**, 046403 (2010).
- [53] F. Evers and A. D. Mirlin, *Rev. Mod. Phys.* **80**, 1355 (2008).

- [54] A. K. Das, A. Ghosh, and I. M. Khaymovich, *Phys. Rev. B* **112**, 024201 (2025).
- [55] M. Janssen, *International Journal of Modern Physics B* **08**, 943 (1994), arXiv:cond-mat/9404015.
- [56] J. Lindinger, A. Buchleitner, and A. Rodríguez, *Phys. Rev. Lett.* **122**, 106603 (2019).
- [57] A. Lakshminarayan, S. Tomsovic, O. Bohigas, and S. N. Majumdar, *Phys. Rev. Lett.* **100**, 044103 (2008).
- [58] See Supplemental Material at [URL will be inserted by publisher] for details which includes [79–92].
- [59] V. E. Kravtsov, I. M. Khaymovich, E. Cuevas, and M. Amini, *New J. Phys.* **17**, 122002 (2015).
- [60] A. K. Das and A. Ghosh, *Phys. Rev. E* **105**, 054121 (2022).
- [61] N. Roy, J. Sutradhar, and S. Banerjee, *Physical Review B* **107**, 115155 (2023).
- [62] M. Schiulaz, E. J. Torres-Herrera, and L. F. Santos, *Phys. Rev. B* **99**, 174313 (2019).
- [63] I. Vallejo-Fabila, A. K. Das, D. A. Zarate-Herrada, A. S. Matsoukas-Roubeas, E. J. Torres-Herrera, and L. F. Santos, *Phys. Rev. B* **110**, 075138 (2024).
- [64] A. K. Das and A. Ghosh, *JSTAT* **2022** (6), 063101.
- [65] A. K. Das and A. Ghosh, *J. Phys. A: Mathematical and Theoretical* [10.1088/1751-8121/ad0b5a](https://doi.org/10.1088/1751-8121/ad0b5a) (2023).
- [66] I. Vallejo-Fabila, A. K. Das, S. Choudhury, and L. F. Santos, *Phys. Rev. E* **112**, 044208 (2025).
- [67] B. Roy, A. K. Das, A. Ghosh, and I. M. Khaymovich, *Phys. Rev. B* **112**, 094206 (2025).
- [68] C. Castelnovo, C. Chamon, C. Mudry, and P. Pujol, *Annals of Physics* **318**, 316 (2005).
- [69] Z. Zhao, M.-A. Filip, and A. J. Thom, *Faraday Discussions* **254**, 429 (2024).
- [70] D. N. Page, *Phys. Rev. Lett.* **71**, 1291 (1993).
- [71] P. Kattel, P. R. Pasnoori, J. H. Pixley, and N. Andrei, *Phys. Rev. B* **111**, 174430 (2025).
- [72] R. Verresen, N. G. Jones, and F. Pollmann, *Phys. Rev. Lett.* **120**, 057001 (2018).
- [73] J. K. Asbóth, L. Oroszlány, and A. Pályi, *A short course on topological insulators*, Vol. 919 (Springer, 2016).
- [74] A. Y. Kitaev, *Physics-uspekhi* **44**, 131 (2001).
- [75] M. Z. Hasan and C. L. Kane, *Rev. Mod. Phys.* **82**, 3045 (2010).
- [76] G. Mahan, *Many-Particle Physics*, Physics of Solids and Liquids (Springer US, 1990).
- [77] T. Giamarchi, *Quantum Physics in One Dimension* (Oxford University Press, 2003).
- [78] A. Pizzi, L.-H. Kwan, B. Evrard, C. B. Dag, and J. Knolle, *Nature Communications* **16**, 6722 (2025).
- [79] D. J. Luitz, I. M. Khaymovich, and Y. B. Lev, *SciPost Phys. Core* **2**, 006 (2020).
- [80] A. K. Das, A. Ghosh, and I. M. Khaymovich, *Phys. Rev. B* **109**, 064206 (2024).
- [81] V. Oganesyan and D. A. Huse, *Phys. Rev. B* **75**, 155111 (2007).
- [82] Y. Y. Atas, E. Bogomolny, O. Giraud, and G. Roux, *Phys. Rev. Lett.* **110**, 084101 (2013).
- [83] A. K. Das and A. Ghosh, *J. Phys. A: Math. Theor.* **52**, 395001 (2019).
- [84] A. K. Das, Validity of generalized gibbs ensemble in a random matrix model with a global \mathbb{Z}_2 -symmetry (2025), arXiv:2506.16176 [cond-mat.stat-mech].
- [85] M. Mehta, *Random Matrices*, Pure and Applied Mathematics (Elsevier Science, 2004).
- [86] A. K. Das, A. Ghosh, and L. F. Santos, *Phys. Rev. B* **111**, 224202 (2025).
- [87] M. Serbyn, Z. Papić, and D. A. Abanin, *Phys. Rev. B* **96**, 104201 (2017).
- [88] P. Sierant, D. Delande, and J. Zakrzewski, *Phys. Rev. Lett.* **124**, 186601 (2020).
- [89] A. L. Corps, R. A. Molina, and A. Relaño, *Phys. Rev. B* **102**, 014201 (2020).
- [90] A. K. Das, C. Cianci, D. G. A. Cabral, D. A. Zarate-Herrada, P. Pinney, S. Pilatowsky-Cameo, A. S. Matsoukas-Roubeas, V. S. Batista, A. del Campo, E. J. Torres-Herrera, and L. F. Santos, *Phys. Rev. Res.* **7**, 013181 (2025).
- [91] A. K. Das and A. Ghosh, *Phys. Rev. E* **106**, 064112 (2022).
- [92] T. Guhr, A. Müller-Groeling, and H. A. Weidenmüller, *Phys. Rep.* **299**, 189 (1998).

Supplementary material

In the Z-basis, the East Hamiltonian in the limit $s \rightarrow -\infty$ has diagonal contributions only from $-\hat{n}_L$, so, 2^{L-1} number of Fock states with L th spin being up have energy -1 . Then, $\text{Tr}\{H\} = 2^{L-1} \times (-1)$. For \hat{H}^2 , the diagonal contributions come from $\mathbb{I} + \sum_{j=1}^L \hat{n}_j^2$ as $(\hat{\sigma}^x)^2 \equiv \mathbb{I}$ such that $\text{Tr}\{\hat{H}^2\} = \text{Tr}\{\mathbb{I} + \sum_{j=1}^L \hat{n}_j^2\} = 2^L + L \times 2^{L-1}$. Then, the 1st and 2nd moments of energy are

$$\langle E \rangle = -\frac{1}{2}, \quad \langle E^2 \rangle = 1 + \frac{L}{2}. \quad (\text{S1})$$

The density of states (DOS) for different system sizes collapse upon the scaling $E \rightarrow \frac{E + \frac{1}{2}}{\sqrt{\frac{L}{2} + \frac{3}{4}}}$. We find that the DOS is well approximated by a Gaussian distribution (Fig. 4).

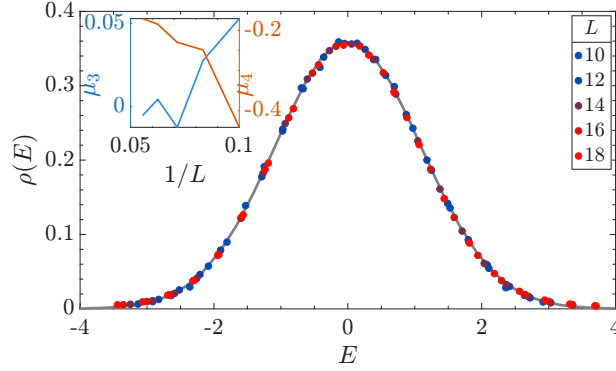


FIG. 4. **DOS for $\hat{H}_{\text{East}}(s \rightarrow -\infty)$** : DOS for different system sizes. The energy axis is centered and scaled to ensure zero mean and unit variance. Grey solid line denotes Gaussian fit. Inset shows the measures of skewness (μ_3) and excess kurtosis (μ_4) as a function of L^{-1} .

Fractal dimensions

To obtain the fractal dimensions, we start from the inverse participation ratios

$$I_q^{(N)} = \sum_{n=1}^N |\Psi(n)|^{2q} \sim N^{(1-q)D_q^{(N)}}. \quad (\text{S2})$$

By extrapolating $D_q^{(N)}$ to infinite system size (assuming that the finite size corrections are polynomial functions of $1/L$ [79, 80]), we extract the fractal dimensions, D_q .

In the Z-basis, the spin-polarized state $|\Theta\rangle = 2^{-L} \left(\frac{1}{\sqrt{3}} \right)^{\otimes L}$ such that the IPRs become

$$I_q^{(N)} = 2^{-2qL} (1 + 3^q)^L \Rightarrow D_q^z = \frac{\log_2(1 + 3^q) - 2q}{1 - q} \quad (\text{S3})$$

Then, for $q \gg 1$, the fractal dimensions of the spin-coherent state can be written as $(\log_2 3 - 2) \frac{q}{1-q}$. In particular, the maximum intensity scales as $\frac{3^L}{2^{2L}}$ such that $D_\infty^z = \log_2 3 - 2 \approx 0.41$. Numerically, we find that $D_\infty^z \approx 0.47$ for the actual ground state.

Following the same procedure as above, we can calculate the fractal dimensions of the spin-coherent state in the

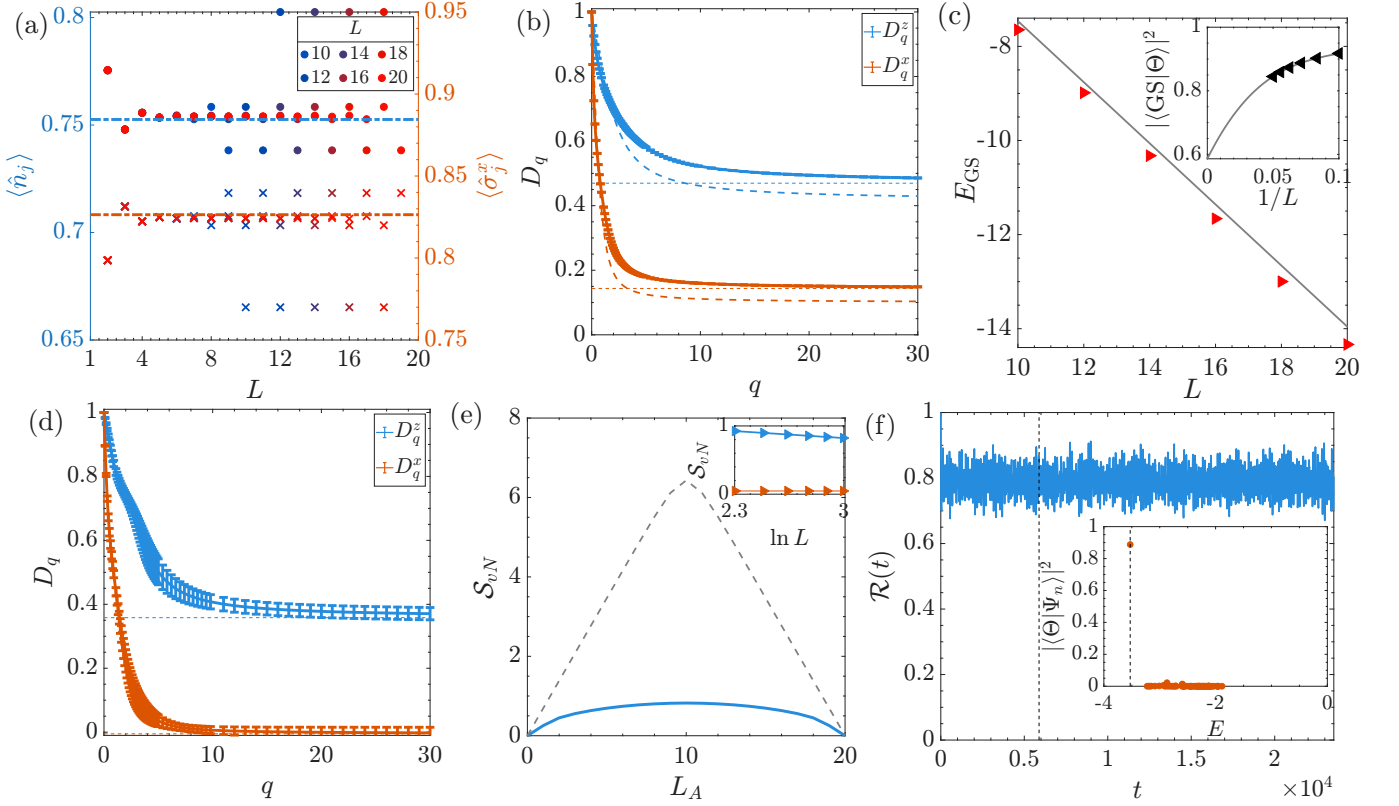


FIG. 5. **Ground state for $\hat{H}_{\text{East}}(s \rightarrow -\infty)$:** (a) Site density (circle) and magnetization in X-direction (cross) w.r.t. ground state for different system sizes shown via different colors. Dashed lines denote the average over the sites and different system sizes. (b) Fractal dimensions of the ground state w.r.t. Z and X bases. Horizontal dotted lines denote D_∞ extracted from the system size scaling of the maximum intensity. Dashed lines denote the fractal dimensions of the spin-coherent state for $\theta = \frac{\pi}{3}$ (Eqs. (S3) and (S4)). (c) Ground state energy as a function of system size via markers while the solid gray line shows the energy of the polarized spin-coherent state, $|\Theta\rangle$. Inset shows the overlap between the ground state and $|\Theta\rangle$. (d) Fractal dimensions of $|\overline{\text{GS}}\rangle$, which is obtained by projecting out $|\Theta\rangle$ from the ground state. (e) von Neumann entanglement entropy of $|\overline{\text{GS}}\rangle$ w.r.t. different subsystem size L_A for $L = 20$. Dashed line denotes the Page curve. Inset shows the entanglement entropy of the ground state (red) and $|\overline{\text{GS}}\rangle$ (blue) for equal bipartition. Solid lines denote linear fit ($1.261 - 1.464 \ln L$ for $|\overline{\text{GS}}\rangle$). (f) Survival probability of $|\Theta\rangle$. Vertical dashed line denotes the Heisenberg time. Inset shows the overlap of $|\Theta\rangle$ with the energy eigenstates where the vertical dashed line denotes the ground state energy. We only show the energy levels for which the overlap is more than N^{-1} .

X-basis, where $|\Theta\rangle = \left(\frac{\sqrt{3}+1}{\sqrt{8}}\right)^L \left(\frac{1}{\sqrt{3}-2}\right)^{\otimes L}$. Corresponding IPRs are

$$\begin{aligned}
 I_q^{(N)} &= \left(\frac{\sqrt{3}+1}{\sqrt{8}}\right)^{2qL} \left(1 + (2-\sqrt{3})^{2q}\right)^L \\
 \Rightarrow D_q^x &= \frac{2\left(\log_2(\sqrt{3}+1) - 3/2\right)q + \log_2(1 + (\sqrt{3}-2)^{2q})}{1-q}
 \end{aligned} \tag{S4}$$

Particularly, the maximum intensity in the X-basis scales as $\frac{(\sqrt{3}+1)^{2L}}{8L}$ such that $D_\infty^x = 3 - 2\log_2(\sqrt{3}+1) \approx 0.10$. Numerically we find that $D_\infty^x \approx 0.14$ for the ground state. In Fig. 7(b), we show the analytical expressions of the fractal dimensions of the spin-coherent state along with those of the ground state in both Z- and X-bases.

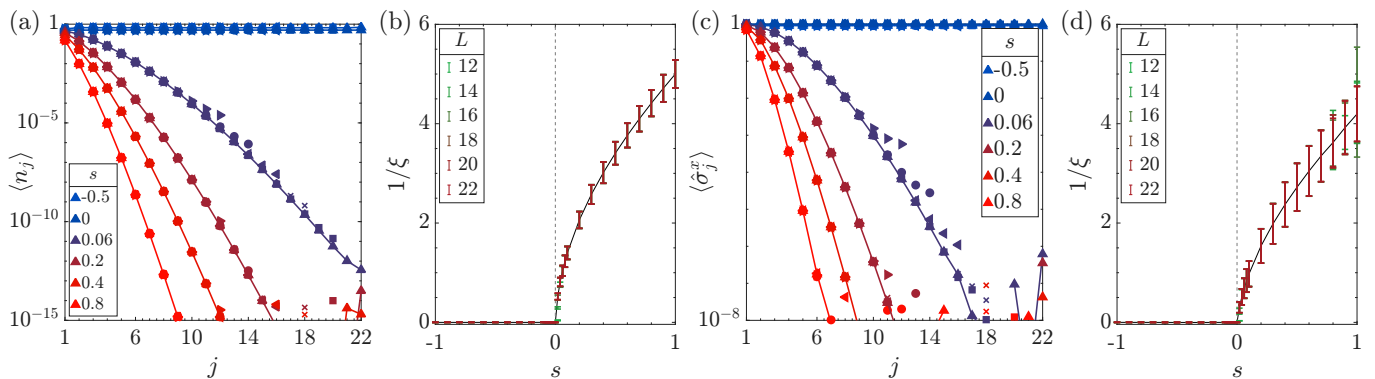


FIG. 6. **Local observables w.r.t. the ground state:** (a) Number density w.r.t. the ground state for different values of s . Makers denote different system sizes, $L = 12, 14, \dots, 22$. (b) The localization length extracted from the exponential decay of the number density w.r.t. lattice sites. (c) Magnetization in the X-direction averaged over the ground state for different values of s . (d) The localization length extracted from the decay of the X-component of the magnetization. Error-bars denote 95% confidence interval.

Ground state localisation for finite s

The single-site occupation $\langle \hat{n}_j \rangle \propto \exp\left(-\frac{j}{\xi}\right)$ where ξ is the real-space localization length. For $s < 0$, $\langle \hat{n}_j \rangle$ in $|GS\rangle$ is a homogeneous function of j [45]. ξ as extracted from the decay of $\langle \hat{n}_j \rangle$ diverges at $s = 0$ approximately as $\xi \sim s^{-\frac{1}{2}}$ (numerically we obtain the exponent to be 0.5481 ± 0.0008 for $L = 22$).

We also compute the expectation value of the magnetization in X-direction, $\langle \hat{\sigma}_j^x \rangle$ w.r.t. the ground state at each lattice site. We observe a similar behavior as that of the number density: for $s < 0$, $\langle \hat{\sigma}_j^x \rangle$ is homogeneously spread over all the lattice sites while for $s > 0$, an exponential decay from the first lattice site is observed, $\langle \hat{\sigma}_j^x \rangle \propto \exp\left(-\frac{j}{\xi}\right)$. For $s = 0$, $\langle \hat{\sigma}_j^x \rangle = 1$ for all values of j as the ground state becomes $|+\rangle^{\otimes L}$. The localization lengths extracted from the exponential decay show power-law divergence at $s = 0$ (for $L = 22$, the numerically obtained exponent is 0.6198 ± 0.0047).

We find that for $s > 0$, $D_q^z = 0$ for any $q > 0$, which implies that the ground state is localized in the Fock space as well as in the real space (reflected in $\langle \hat{n}_j \rangle$ vs. j). On the other hand, for $s < 0$, we find that $0 < D_q^z < 1$ for all values of $q > 0$ and $D_q^z > D_{q'}^z$ for $q < q'$. Thus, the ground state of the East model is multifractal over the Z-basis for $s < 0$, despite being homogeneously spread over the real space.

As opposed to the Z-basis, we find the ground state to be uniformly spread over all the X-basis states for $s > 0$, as reflected by $D_q^x = 1$ for all values of q . This is expected as a product state in Z-basis is completely extended in the X-basis. On the other hand, the ground state is multifractal in X-basis for $s < 0$ where the fractal dimensions are bounded by $0 < D_\infty^x < 1$. Thus, by looking at the fractal dimensions of the ground state, we are able to identify the QPT at $s = 0$.

We find that $D_\infty^x \rightarrow 0$ and $D_\infty^z \rightarrow 1$ for $s \rightarrow 0$, as shown in Fig. 7(c). Previously, we saw that $\langle \hat{n}_j^x \rangle = 1$ w.r.t. the ground state for all the lattice sites at $s = 0$. This conclusively shows that the ground state of the East model is $|+\rangle^{\otimes L}$ at $s = 0$, being completely extended (localized) in the Z-basis (X-basis). This is also reflected in the bipartite von Neumann entanglement entropy of the ground state, which goes to zero at $s = 0$ and exhibits a discontinuity, as shown in Fig. 7(d). For all values of s , the entanglement entropy of the ground state remains much smaller than the Page value observed in case of the maximally entangled states [70].

Energy correlations for $s \rightarrow -\infty$

Above analyses raise the question: are all the bulk states (away from the spectral edges containing $\mathcal{O}(1)$ states) ergodic? If yes, then all such bulk states strongly hybridize with each other and leads to correlated energy levels in the middle of the spectrum. Thus, to probe ergodicity in our system, first, we look at the energy correlations. To quantify the nature of short-range correlations (on the scale of mean level spacing), we look at the ratio of level spacing [81–84].

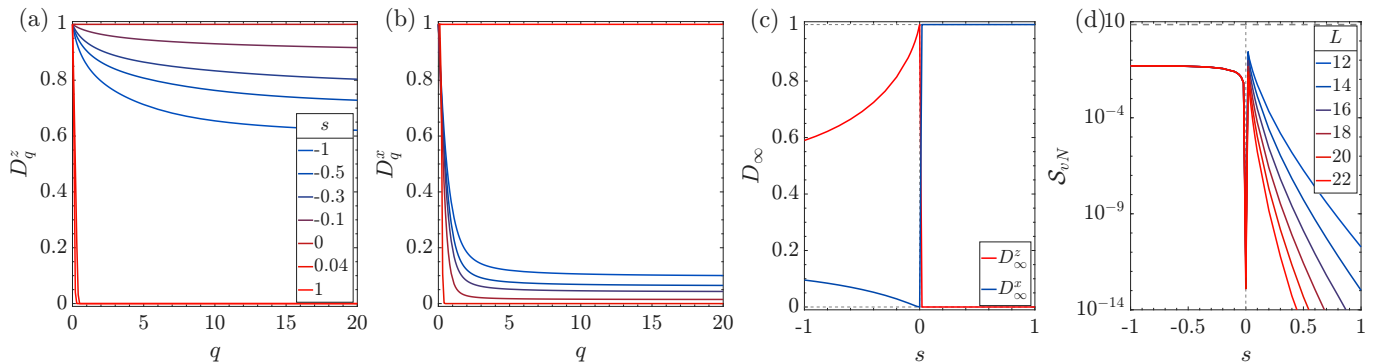


FIG. 7. **Fractal dimensions of the ground state:** Fractal dimensions w.r.t. (a) Z-basis and (b) X-basis for various values of s . (c) D_∞ obtained from the system size scaling of the maximum intensity in both Z- and X-bases. (d) Bipartite von Neumann entanglement entropy of the ground state for different system sizes. The horizontal dashed line denotes the Page value for $L = 20$.

The average ratio of level spacing is approximately 0.53 (0.39) for the GOE (Poisson ensemble). We find that for the East Hamiltonian at $s \rightarrow -\infty$, the average ratio of level spacing is approximately 0.53 and corresponding distribution follows the analytical expression of that of the GOE, as shown in the inset of Fig. 8(a). Thus, nearby bulk energy levels are strongly correlated as in random matrix theory.

The presence of short-range correlation however does not guarantee that two energy levels with gap much larger than the mean level spacing are correlated, which is expected in an ergodic system. To probe such long-range correlation, we look at the level number variance [67, 84–86]. In case of GOE, where all the energy levels are correlated, the number variance exhibits a logarithmic behavior. Contrarily, the number variance is linear in case of the Poisson ensemble, where any two energy levels are uncorrelated. In physical systems, there may exist a mesoscopic energy scale called the Thouless energy, which is typically smaller (larger) than the global energy bandwidth (mean level spacing) [64, 86–91]. Energy levels with gap smaller than the Thouless energy are correlated similar to the random matrix models whereas energy correlations cease to exist on a larger energy scale.

To compute the number variance, it is necessary to unfold the energy spectrum to get rid of the model dependent global trend of the DOS such that mean level spacing becomes unity [92]. We denote the unfolded energy levels as \mathcal{E} . In Fig. 8(a), we show the level number variance of the East model in the $s \rightarrow -\infty$ limit averaged over energy windows of length $\Delta\mathcal{E}$ and centers over the middle 50% of the spectrum. We identify the Thouless energy as the energy scale above which the number variance deviates from that of the GOE. For $L = 14$, the Thouless energy is $\sim \mathcal{O}(10)$, which is larger than the mean level spacing ($\mathcal{O}(1)$) but much smaller than the global bandwidth ($\mathcal{O}(N)$). Thus, extensively large number of energy levels in the bulk spectrum are weakly correlated or uncorrelated unlike the typical ergodic systems.

To understand the manifestation of the Thouless energy in the middle of the spectrum, we obtain middle 256 eigenstates for different system sizes. In Fig. 8(b), we show the fractal dimensions in the Z-basis averaged over the middle 256 eigenstates. We find that $D_q \approx 1$ for all values of q as expected in ergodic states. This is also reflected in the von Neumann entanglement entropy, which exhibits volume law growth, as shown in the inset of Fig. 8(b). To capture the degree of hybridization among the eigenstates, we look at the overlap [59]

$$K(\omega) = N \sum_{n=1}^N |\Psi_E(n)|^2 |\Psi_{E+\omega}(n)|^2 \quad (S5)$$

where $N = 2^L$ is the Hilbert space dimension, $|\Psi_E\rangle$ is the eigenstate with energy E . $K(\omega) \approx 1$ for two eigenstates with strong overlap as in the ergodic systems whereas a power-law decay is observed for $\omega > E_{\text{Th}}$. In Fig. 8(c), we show the overlap as a function of energy gap for middle 256 eigenstates. We find that $K(\omega) \approx 1$, i.e. all such states are strongly hybridizing. To support this conclusion, we also look at the spectral function of a local observable [87]

$$f^2(\omega) = e^{S(E)} \sum_{m,n} |\mathcal{O}_{mn}|^2 \delta(\omega - |E_m - E_n|) \quad (S6)$$

where $S(E)$ is the thermodynamic entropy at $E \equiv (E_m + E_n)/2$ and $\mathcal{O}_{mn} \equiv \langle \Psi_{E_m} | \hat{\mathcal{O}} | \Psi_{E_n} \rangle$. We consider the entropy to be $S(E) = \ln(N\rho(E))$, where $\rho(E)$ is the DOS and take the local observable to be $\hat{n}_{L/2}$. In Fig. 8(c), we show

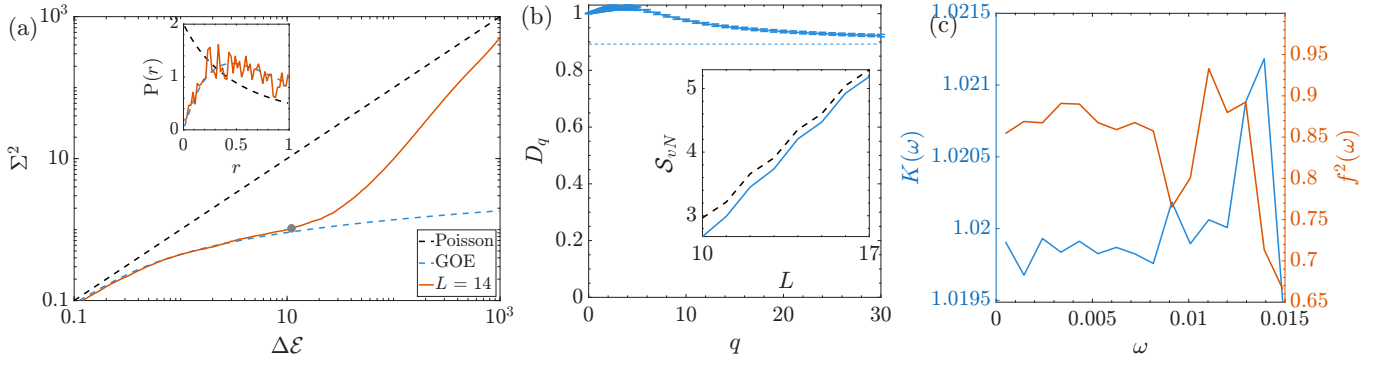


FIG. 8. $\hat{H}_{\text{East}}(s \rightarrow -\infty)$: (a) Number variance for $L = 14$ averaged over energy windows with centers in the middle 50% of the spectrum. Dashed lines denote the analytical expressions of the Poisson and GOE. Marker denotes the Thouless energy. Inset shows the density of the ratio of level spacing along with the analytical expressions of the Poisson and GOE. (b) Fractal dimensions averaged over middle 256 eigenstates for $L = 17$. Inset shows the entanglement entropy averaged over middle 256 eigenstates as a function of system size. Black dashed line denotes the Page values. (c) Overlap of the eigenstates and spectral function vs. energy gap for $L = 17$.

that the spectral function is also homogeneous for the middle 256 states. Thus, the eigenstates in the middle of the spectrum typically behave as ergodic wavefunctions.